J Mater Sci (2008) 43:4945–4952
DOI 10.1007/s10853-008-2723-x

Delayed hydride cracking velocity in Zr-2.5Nb: detection by acoustic emission and theoretical model testing

J. I. Mieza · G. Vigna · E. Chomik · G. Domizzi

Received: 20 February 2008 / Accepted: 12 May 2008 / Published online: 3 June 2008

Abstract Acoustic emission (AE) detects elastic waves generated during delayed hydride cracking (DHC). The detection of the first acoustic signal is used to measure the propagation time. This time and the crack length measured on the broken specimen are used to determine the DHC velocity. In this work, DHC tests were carried out on Zr-2.5Nb alloy from CANDU pressure tubes. Linear relationship between cumulative count rate and cracking velocity was corroborated. It is generally accepted that the hydrides crack when they reach a critical length; nevertheless, in this work the number of signals generated during typical DHC test were higher than expected from that assumption. Dutton and Puls DHC model with some parameters calculated by Shmakov et al. was used to test out against experimental data. This modification is an original approach that makes more rational the DHC velocity calculation, avoiding arbitrary parameter selection. Good agreement was obtained for two different CANDU pressure tubes.

J. I. Mieza (✉) · G. Vigna · E. Chomik · G. Domizzi
Unidad de Actividad Materiales, Centro Atómico Constituyentes, Comisión Nacional de Energía Atómica, Av. Gral. Paz 1499, (B1650KNA) San Martín, Buenos Aires, Argentina
e-mail: mieza@cnea.gov.ar

J. I. Mieza
CONICET (Consejo Nacional de Investigaciones Científicas y Técnicas), Buenos Aires, Argentina

Introduction

Zr-2.5Nb pressure tubes (PT) in CANadian Deuterium Uranium (CANDU) nuclear power plants are susceptible, under certain conditions of hydrogen concentration, stress gradient, and temperature, to a degradation mechanism known as delayed hydride cracking (DHC) [1, 2]. This mechanism acts repetitively in discrete steps creating a growing crack. One of the most important parameters used for DHC characterization is the velocity of crack propagation (V_p), as this value is necessary to determine the available time before catastrophic crack when leak before break (LBB) criterion is applied [3]. In DHC test, V_p can be estimated in a destructive way by measuring the length of fracture surface over time of propagation. However, as hydride fractures occur inside the specimen, a nondestructive technique, such as direct current potential drop (DCPD) [4] or acoustic emission (AE) [5], is necessary to detect the precise moment when DHC starts. We choose the AE method because its temperature dependence is negligible [5], and it can detect—in appropriate configuration—both, plastic deformation and brittle crack [6].

Acoustic emission is a dynamic process of generation and propagation of elastic waves within a material in an ultrasonic range [7]. In metals, acoustic emission has been identified from a broad range of sources, from avalanches of dislocations to fracture and decohesion of second phase precipitates [6]. During DHC process, acoustic emission signals are mainly generated by brittle hydride fractures and propagate within the solid. Acoustic signal is then transformed into an equivalent electric signal by means of piezoelectric transducer; Fig. 1 shows an AE signal and its typical parameters. Further electronic conditioning and processing of signals are needed to extract useful information. Although AE technique has been demonstrated to

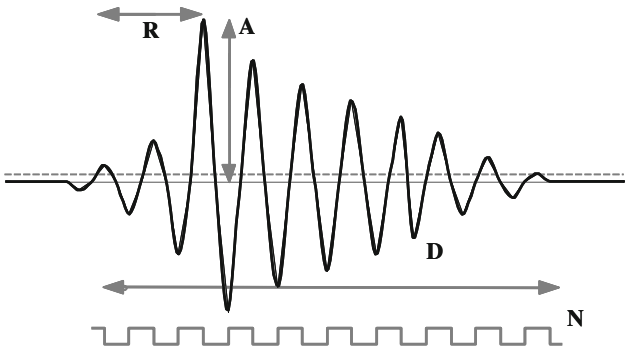

Fig. 1 Typical parameter definition of AE event. A, amplitude; R, rise time; D, duration; N, counts. Dashed line represents threshold level

be useful for detecting DHC start, there are controversial opinions about the feasibility of using AE to measure DHC velocity. Arora and Tangri [8] state that "AE is a viable technique for determining the crack velocity," while Lin et. al. [9] manifest "Because of the large scatter in the AE, there is no quantitative measure possible of crack advance...." Our goal was to elucidate if any acoustic emission parameter is reliable to estimate DHC velocity during a test.

On the other hand, since three decades ago great efforts have been devoted in order to model DHC process for prediction and diagnosis [10–16]. The modeling strategy was based on the steady-state solution of the hydrogen diffusion equation in the presence of stress gradient [10, 11]. DHC velocity is calculated with a relationship (Eq. 1) which depends, basically, on the hydrogen diffusion coefficient (D_H), and the hydrogen solubility (E) at the crack tip-hydride location (l) and at the surrounding bulk hydride location (L) [11].

$$V_p = f(D_H, t_h \ldots)(E(L) - E(l)) \quad (1)$$

This relationship has been successfully correlated with experimental data measured in PT from different metallurgical states [10, 17, 18]; nevertheless, some parameters—like hydride thickness t_h, l, and L—were chosen with different criteria. For example, t_h and L were usually taken from experimental data, l was calculated as the position of maximum hydrostatic stress [11, 14] or equated to the striation length measured on the fracture surface [18]. Recently, Shmakov et al. [16] presented an integrated model which combines the hydrogen diffusion equation with critical characteristics of hydrides (thickness and length) depending on temperature and stress intensity factor.

In this work, crack velocity was measured in a CANDU Zr-2.5Nb PT, in the range of reactor temperature. New acoustic emission data related to DHC process are presented. Also, the theoretical model of DHC phenomena [11] with l, L, and t_h parameters calculated by Shmakov et al. [16] was tested out against experimental data.

Experimental

DHC measurements were carried out with curved compact toughness (CCT) samples according to the guidelines of IAEA Round Robin [19]. The material was a nonirradiated section of CANDU Zr-2.5Nb pressure tube of Embalse Nuclear Power Plant. Samples were previously hydrided to a concentration of about 50 and 80 ppm of hydrogen in a Sieverts device, and then heat-treated for hydride homogenization during 7 days at 380 °C. Figure 2 shows the layout of the used device.

Crack propagation was monitored by acoustic emission. Two wide band piezoelectric sensors were selected for signal characterization in order to get the broadest spectrum possible. The main sensor was attached to a Zr-2.5Nb wave-guide, out of the high-temperature zone, and the wave-guide was fixed to the sample by resistance welding. A second "guard" sensor was attached to the structure of the tension machine in order to filter spurious noise. Each AE transducer was connected to a 40 dB preamplifier and to a band pass filter in the range 0.1–1 MHz. The preamplified and filtered signal was subsequently amplified 25 dB, analyzed for parameter extraction, and digitized at 5 MSamples/s. The AE signal, to be computed as a true

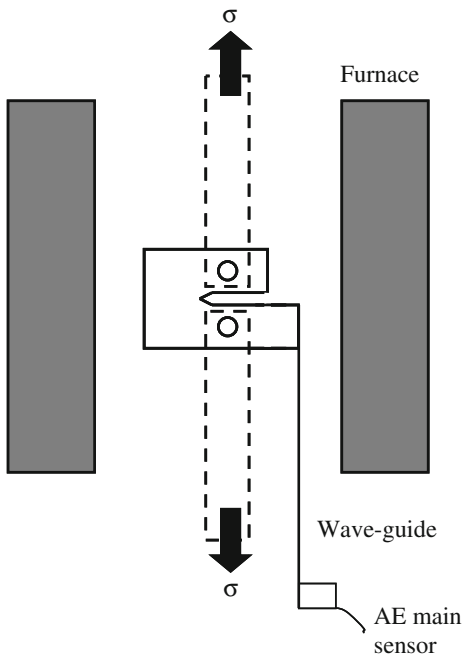

Fig. 2 Layout of employed device. Samples inside a furnace are loaded with initial $K_I = 15$ MPa m$^{1/2}$. Wave-guide and acoustic emission sensor are attached for the detection of DHC phenomenon

delayed hydride cracking event, must be higher than the threshold value, settled 2.5 times higher than the electronic noise of the measurement system. Propagation time is measured from the detection of the first DHC event.

In order to produce a sharp crack at notch tip, CCT specimens were fatigue pre-cracked [19]. The pre-cracking length was about 2 mm in each sample. Fatigue cracking was performed in two steps: the first one with a maximum stress intensity factor K_I of 19 MPa $m^{1/2}$ and cyclic loads from 1.58 to 0.158 kN, and the second one with a maximum K_I factor of 10 MPa $m^{1/2}$ and cyclic loads from 1.071 to 0.01071 kN.

Each test was subjected to a temperature cycle as the one shown in Fig. 3. The cycle consisted of a heating ramp up to a temperature where all hydrides were dissolved; then cooling down to test temperature, where precipitated hydrides and hydrogen in solution coexisted [19]. After holding 1 h at test temperature, a constant load was applied to produce an initial $K_I = 15$ MPa $m^{1/2}$ which assures a constant DHC velocity [2]. At the end of each DHC test, samples were unloaded and cooled down to room temperature. Finally, specimens were broken opened in two halves by applying an overload.

DHC velocity was calculated in postmortem specimens by measuring the length of fracture surface using the nine lines method [20] and using the propagation time. The same mechanical and acoustic configuration was maintained during all tests in order to minimize the variability in the measurements.

Characterization of Nb percentage of β phase was made by X-ray powder diffraction. Powder was obtained by electrolytic anodic dissolution of α phase in a methanol, perchloric acid and butoxyethanol solution [21]. For X-ray diffraction, Cu-Kα radiation was used, in the range 10–70° of 2θ, with scanning step of 0.02° every 15 s.

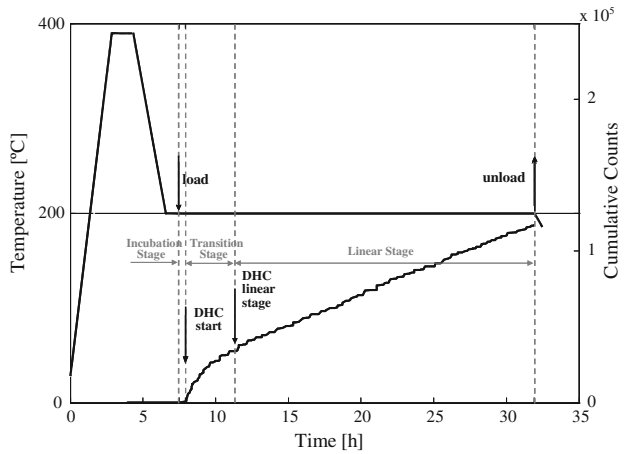

Fig. 3 Typical temperature cycle and cumulated count from AE events

Results and discussion

Five different temperatures in the range of reactor operation were chosen for testing the samples. Table 1 shows the details of each test and Fig. 4 shows a typical DHC fracture surface.

A dummy sample, without hydrogen, was first tested to characterize the acoustic behavior of the system. No significant signals, than the background electronic noise, were observed.

DHC velocities versus temperatures are plotted in Fig. 5. The same figure shows other authors' [22] values measured on another as fabricated CANDU PT, without any subsequent thermomechanical treatment. These values are higher than those measured in this work. Table 2 shows a comparison between the mechanical properties of both materials.

It is known that thermal history affects DHC velocity [23, 24] by changing the alloy strength, and the composition and morphology of metastable β-Zr phase. The metastable phase β-Zr (20% Nb) transforms to equilibrium β-Nb ($\sim$85 wt% Nb) phase, passing through intermediate stages with metastable ω phase precipitation and Nb enrichment of β-Zr [25].

The Nb percentage of β phase (β-Zr*) can be evaluated by measuring lattice parameter (a_β) in X-ray diffraction diagrams according to Eq. 2 [26].

$$a_\beta[\text{Å}] = 3.588 - 0.002888x \ (\text{wt\% Nb}) \tag{2}$$

Figure 6 shows the position of (110) diffraction peak of PT tested in this work which corresponds to $\sim$70% of Nb in β phase. At temperatures higher than 300 °C, the β phase transformation slows down DHC velocity as the transformation progress [24]. The lower DHC velocity measured in this work is in agreement with the high Nb percentage ($\sim$70%) in β phase compared with ($\sim$20–50%) [27] in typical CANDU PT similar to that used in the IAEA Round Robin [22]. According to Ref. [25] a heat treatment at 380 °C during 168 h explains the $\sim$70% of Nb in β phase. It is expected that heat treatment not only increases the Nb percentage of β phase but also cuts the continuity of the β lath [24], produced during the PT extruding. Subsequently, this transformation of β phase produces a decrease in hydrogen diffusion coefficient [28].

Figure 5 also shows a DHC velocity fitting of the experimental data according to Puls's model [10, 11], Eq. 3.

$$V_p = \frac{2\pi D(E(L) - E(l))}{(\Omega_{Zr}\Phi(L,l)t_h N_H x)} \tag{3}$$

where $E(l)$ and $E(L)$ are the terminal solid solubility of hydrogen in the presence of applied stresses near and far away from the crack tip, respectively. These variables (as

Table 1 Conditions and results of DHC tests

Test no	Hydrogen concentration (ppm)	Test temperature (°C)	K_I (initial) (MPa $m^{1/2}$)	Crack length (m)	Test time (s)	V_p DHC velocity (m/s)	dN_c/dt (counts/s)
1	80	259	15.0	7.36E-4	12,600	5.85E-08	20.93
2	80	232	13.3	4.43E-4	25,200	1.76E-08	5.95
3	50	220	15.4	6.03E-4	38,376	1.57E-08	4.41
4	50	200	15.9	7.13E-4	87,898	8.12E-09	1.10
5	50	180	16.3	9.34E-4	218,700	4.27E-09	0.37

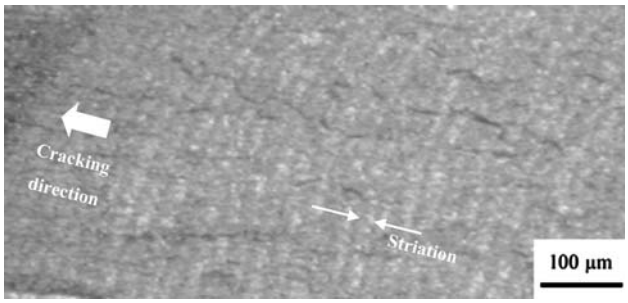

Fig. 4 Typical DHC fracture surface. Striations are perpendicular to cracking direction

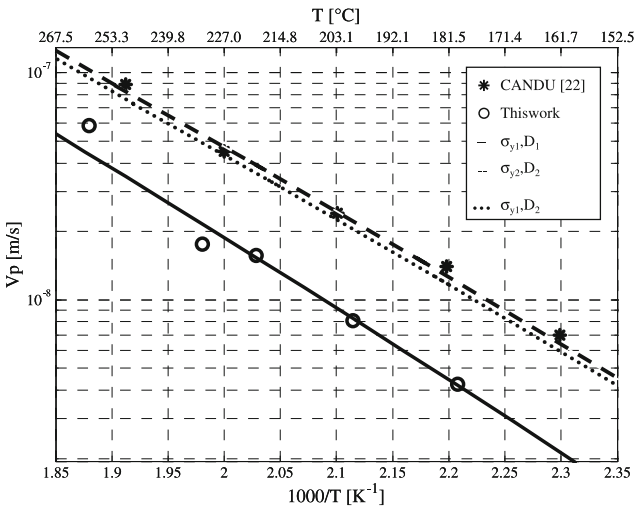

Fig. 5 DHC velocity versus temperature. Experimental data and model fitting of typical CANDU (average of [22]) and this work PTs

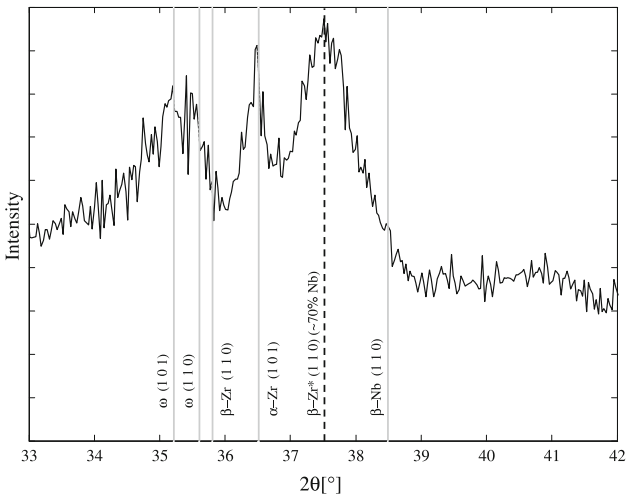

Fig. 6 Powder X-ray diagram of this work PT. The peak (1 1 0) of β-Zr phase is shifted to higher angles due to an increase in Nb concentration

defined in [18]) and other parameters of Eq. 3 are shown in Table 3.

The hydrogen diffusion coefficient measured by Skinner and Dutton [28], in the axial direction, for an autoclaved PT (400 °C/24 h) was selected for the PT used in the IAEA RR [22], which was tested in the same condition .For the heat treatment received by the material used in this work (autoclaved 400 °C/24 h + 380 °C/168 h), there is no hydrogen diffusion coefficient reported in literature. Skinner and Dutton [28] measured hydrogen diffusion after heat-treating at 400 °C during 24 h an autoclaved PT. For a similar heat treatment (400 °C/48 h), Griffiths et al. [25]

Table 2 Mechanical properties of materials

Material	Test temperature (°C)	0.2% Yield stress (MPa)[a]	Micro hardness [HV0.2][b]
IAEA Round Robin [22]	20	803	272.7
	250	567	–
This work (as received: 400 °C/24 h)[c]	20	705 ± 39.5	214.5 ± 2.1
	250	507 ± 37.6	–
This work (380 °C/168 h)	20	–	219 ± 5.5
	250	–	

[a] Tensil axis parallel to PT circumferential direction

[b] Measured in RC plane of pressure tube

[c] CNEA private report

Table 3 Definition of parameters and variables used in Eq. 3

V_p:	DHC velocity (m/s)
l:	Distance from crack tip to hydride tip
L:	Distance away from the hydride tip
$E(l)$ =	$TSSP1 \cdot e^{\overline{W}_t^a(l)/RT}$
$E(L)$ =	$TSSP2 \cdot e^{\overline{W}_t^a(L)/RT}$
$TSSP1$:	Equilibrium hydrogen concentration at hydride tip during precipitation (without memory effect, cooling from 420 to 450 °C [29])
$TSSP2$:	Equilibrium hydrogen concentration away from hydride tip during precipitation (with memory effect, cooling from 220 to 368 °C [29])
$\Phi(L, l)$ =	$\int_l^L \exp(p(r)\overline{V}_H/RT)\mathrm{d}r/r$
$p(r)$ =	$\sigma_{ii}/3$, hydrostatic stress at r
$\overline{W}_t^a(L,l)$ =	$-\overline{V}_{hid}\sigma_{ij}e_{ij}$, total interaction energy per mole of H due to hydride formation under external stress (summation over repeated indices i, j = 1,2,3)
σ_{ij} :	Applied external stress. Under plain strain conditions holds [11]
	At l $\sigma_{11} = 3.35\sigma_y$, $\sigma_{22} = 2.08\sigma_y$, $\sigma_{33} = 2.71\sigma_y$
	At L $\sigma_{11} = \sigma_{22} = K_I/\sqrt{2\pi L}$ and $\sigma_{33} = 2\nu K_I/\sqrt{2\pi L}$
e_{ij}:	Hydride (stress-free) transformation strains [30]
	At l $e_{22}^T = e_{33}^T = 0.0458, e_{11}^T = 0.072$
	At L $e_{11}^T = e_{33}^T = 0.0458, e_{22}^T = 0.072$
	At the crack tip, the normal-to-hydride platelet is parallel to circumferential direction of PT and applied stress, while at L the normal-to-hydride platelet is parallel to radial direction of PT
$\overline{V}_H$ =	16.7×10^{-7} (m^3/mol), molal volume of hydrogen [31]
$\overline{V}_{hid}$ =	16.3×10^{-6} (m^3/mol hydride), hydride volume per mole H [30]
D_1 =	$3.5 \times 10^{-7} e^{(-39558/RT)}$ (m^2/s), hydrogen diffusion coefficient in Zr-2.5Nb heat-treated 24 h at 400 °C after autoclaved at 400 °C during 24 h [28]. Used for this work experimental data
D_2 =	$2.4 \times 10^{-7} e^{(-34700/RT)}$ (m^2/s), hydrogen diffusion coefficient in autoclaved Zr-2.5Nb [28]. Used for typical CANDU PT [18, 22]
σ_{y1} =	(957 − 0.86 T) (MPa), extrapolated yield stress from CANDU PT of Embalse Nuclear Power reactor (this work)
σ_{y2} =	(1103.6 − 1.026 T) (MPa), extrapolated yield stress for CANDU RX04 PT [18, 22]
R =	8.314 (J/mol K), universal constant of gases
N_H =	6.13×10^{28} ($atom/m^3$), atomic density of zirconium hydride [11]
x =	1.66 (at. H/at. Zr), hydrogen atoms in the hydride ZrHx
Ω_{Zr} =	2.3×10^{-29} (m^3/atom), atomic volume of zirconium [30]
T:	Temperature (K)

obtained around 64% of Nb in β phase. As this value is approximately similar to the 70% of Nb obtained in this work material, the value reported in Ref. [28] was used for V_p calculation. The hydrogen diffusion coefficients are reported in Table 3.

From the yield stress data reported in Table 2, two linear regressions were obtained for the material employed in this work ($\sigma_{y1} = 957 - 0.86\ T$ MPa), and that one used in the IAEA Round Robin [22] ($\sigma_{y2} = 1103.6 - 1.026\ T$ MPa). As is shown in Table 2 the heat treatment received by this work material did not affect the microhardness; then, it is expected that the yield stress did not change either.

The expressions for the distances from the crack tip were taken from [16] as $l = r_m + l_c$ and $L = 20r_p$, where r_m is the location of maximum stress from the crack tip, l_c is the critical length of hydride, and r_p is the radius of plastic zone at the crack tip.

$$r_m = \frac{(1-2\upsilon)^2}{6\pi}\left(\frac{K_{IC}^{\delta}}{\sigma_y}\right)^2 [\mu m] \quad (4)$$

$$l_c = \frac{(1-2\upsilon)^2}{6\pi}\left(\frac{K_{IC}^{\alpha} - K_I}{K_I - K_{IC}^{\delta}}\right)\left(\frac{K_I}{\sigma_y}\right)^2 [\mu m] \quad (5)$$

$$r_p = \frac{(1-2\upsilon)^2}{2\pi}\left(\frac{K_I}{\sigma_y}\right)^2 [\mu m] \quad (6)$$

Parameters of Eqs. 4 and 5 are defined in Table 4.

Finally, hydride thick (t_h) was calculated according to [16] as

$$t_h = \frac{2K_{IC}^{\delta}(1-\upsilon^2)(1-2\upsilon)\left[4\sigma_y - 3(1-2\upsilon)\sigma_{fh}\right]}{9E\varepsilon_{\perp}\sigma_y^2} [\mu m] \quad (7)$$

where $\varepsilon_{\perp}$ is the hydride (stress free) transformation strain that, for an anisotropic material, holds $\varepsilon_{\perp} = 0.0458 + 0.0262 f_T$ [33], and $f_T = 0.62$ is the fraction of α zirconium

Table 4 Definition of variables and parameters used in Eqs. 4–7

$v = 0.436 - 4.8 \times 10^{-4}$ (T-273) Poisson's ratio [11]
$K_I = 15$ (MPa $m^{1/2}$), stress intensity factor
$K_{IC}^{\delta} = 5.35$ (MPa $m^{1/2}$), fracture toughness for delta hydride [16]
$K_{IC}^{\alpha} = 45$ (MPa $m^{1/2}$), fracture toughness for alpha phase [16]
$\sigma_{fh} = 650.84 - 0.09096\ T$ (MPa), fracture strength of zirconium hydride [32]
$E = 95.9 - 0.0574$ (T-273) (GPa), elastic modulus [11]

grains whose normal to the {0001} basal planes lies in the circumferential direction.

Good agreement was obtained between experimental data and the velocity calculated with the yield stress and hydrogen diffusion coefficient reported in Table 3. In order to evaluate if the lower strength of this work material might explain by itself the lower DHC velocity measured, V_p was re-calculated using the diffusion coefficient D_2 and the yield stress σ_{y1} (Fig. 5). No significant velocity reduction was obtained, showing that the strength effect is negligible compared with the diffusion effect.

In Fig. 3, cumulative counts of AE events generated during a test are superposed to the temperature cycle. The cumulative count curve shows three distinct stages [8]: an incubation stage where no AE is detected, a transition stage with high cumulative count rate (dN_c/dt), and finally a linear behavior. This last stage count rate is correlated with the velocity of DHC propagation (V_p) measured in postmortem specimens (Fig. 7). It was found a linear correlation, Eq. 8, between acoustic emission cumulative count rate and DHC velocity over the temperature range studied, with a linear correlation index R over 0.98.

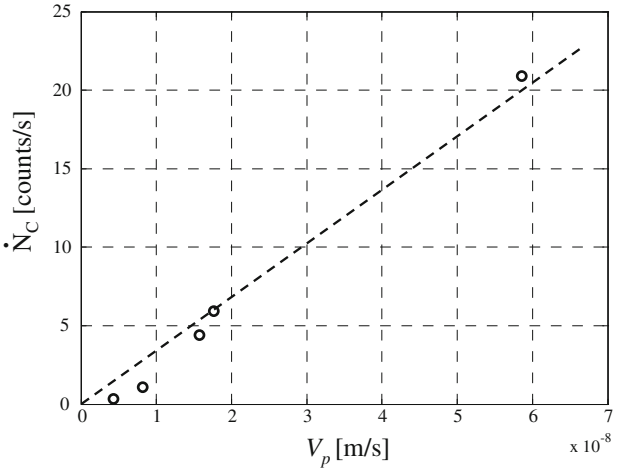

Fig. 7 Linear correlation between DHC velocity and AE cumulative count rate

$$V_p\ [\mathrm{m/s}] = 3 \times 10^8 dN_c/dt \tag{8}$$

This relationship may be used as a nondestructive tool for DHC velocity estimation during tests, provided that the same acoustic configuration is settled.

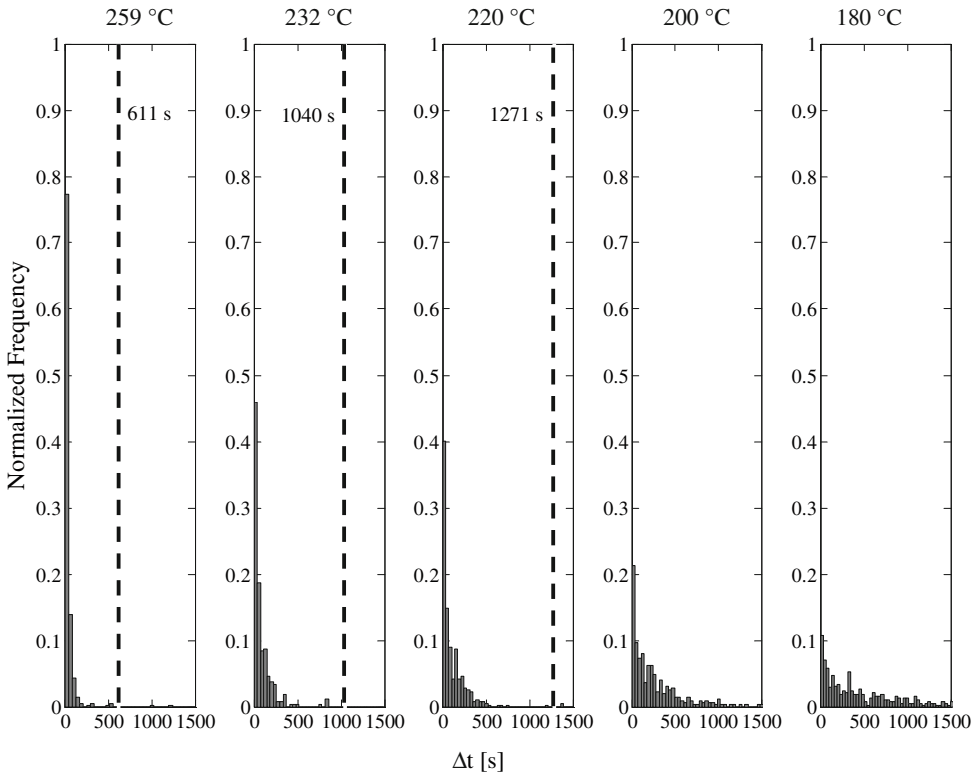

Fig. 8 Experimental inter-event time histograms. Dashed lines indicate the theoretical time between hydride fractures, assuming one signal every l_c step. For 200 and 180 °C test, calculated time is beyond the scale

Table 5 Calculated critical time for hydride fracture

Temperature (°C)	259	232	220	200	180
Critical time (s)	611	1040	1271	1977	3267

The number of acoustic emission signals generated during DHC tests has been proposed to be approximately equal to the number of striations in fracture surface and each striation produced by a cracked hydride [9, 34] (see Fig. 4). However, there are evidences [8] that the number of signals generated during a typical DHC test is higher than the number of striations; this may be a consequence of a complex fracture pattern inside a striation [35]. Our data support the latter hypothesis as shown in Fig. 8, where a theoretical calculation of time for critical length fracture is compared with the histogram of times between successive AE events. The theoretical time is calculated as the ratio of l_c [16] over V_p from Eq. 3 and shown in Table 5. The histogram represents the number of AE events separated from the next one by a time interval of $n\Delta t$, for $\Delta t = 40$ s and $n = 25$. Figure 8 shows that acoustic emission occurs more frequently than the time required for reaching the critical length, suggesting that one crack per critical hydride length is a rough simplification.

Conclusions

In this work we apply acoustic emission technique to evaluate delayed hydride cracking of nonirradiated Zr-2.5Nb alloy from CANDU pressure tube.

We found a linear relationship between acoustic emission cumulative count rate and DHC velocity over the range of test temperatures (180–259 °C). This relationship allows to estimate online DHC velocity in a nondestructive way.

The material used in this work presents lower DHC velocity than typical CANDU tubes; this can be explained by the high degree of decomposition of metastable β-Zr phase, which slows down hydrogen diffusion. This fact was tested out with a theoretical model of DHC velocity prediction, showing that hydrogen diffusion coefficient is the key parameters for a good fitting.

From inter-events time histograms of experimental AE signals, the number of signals generated during typical DHC test proves to be higher than that expected by the fracture model of one crack every time the hydride reaches its critical length.

Acknowledgements We would like to thank GOE (Elastic Wave Group) of CNEA for its assistance in acoustic emission technique.

References

1. Coleman CE, Ambler JFR (1979) Rev Coat Corros III(2 & 3): 105–157
2. Simpson LA, Puls MP (1979) Metall Trans A 10A:1093–1105. doi:10.1007/BF02811655
3. Moan GD, Coleman CE, Price EG, Rodgers DK, Sagat S (1990) Int J Press Vessels Pip 43:1–21. doi:10.1016/0308-0161(90)90089-Z
4. Simpson LA, Clarke CF, Atomic energy of Canada Limited AECL-5815
5. Sagat S, Ambler JFR, Coleman CE, Atomic energy of Canada Limited AECL-9258
6. Heiple CR, Carpenter SH (1987) J Acoustic Emission 6(3):177–204
7. Scruby CB (1987) J Phys E 20:943–953. doi:10.1088/0022-3735/20/8/001
8. Arora A, Tangri K (1981) Int Adv NDT 8:217–236
9. Lin G, Skrzypek S, Li D, Eadie RL (1998) J Test Eval 26(1): 15–25
10. Dutton R, Nutall K, Puls MP, Simpson LA (1977) Metall Trans A 8A:1553–1562
11. Puls MP (1990) Metall Trans A 21A:2905–2917. doi:10.1007/BF02647211
12. Shi S-Q, Liao M, Puls MP (1994) Model Simul Mater Sci Eng 2:1065–1078
13. Lufrano J, Sofronis FP, Birnbaum HK (1996) J Mech Phys Solids 44(2):179–205. doi:10.1016/0022-5096(95)00075-5
14. Sagat S, Chow CK, Puls MP, Coleman CE (2000) J Nucl Mater 279:107–117. doi:10.1016/S0022-3115(99)00265-2
15. Ma XQ, Shi SQ, Woo CH, Chen LQ (2006) Mech Mater 38:3–10. doi:10.1016/j.mechmat.2005.05.005
16. Shmakov AA, Singh RN, Yan D, Eadie RL, Matvienko YG (2007) Comput Mater Sci 39:237–241. doi:10.1016/j.commatsci.2006.02.022
17. Sagat S, Coleman CE, Griffiths M, Wilkins BJS (1994) In: Garde AM, Bradley ER (eds) Zirconium in the nuclear industry: 10th Int. symposium, ASTM STP 1245. ASTM, Philadelphia, pp 35–39
18. Cirimello P, Domizzi G, Haddad R (2006) J Nucl Mater 350:135–146. doi:10.1016/j.jnucmat.2005.12.002
19. Choubey R, AECL report no. FC-IAEA-02 T1.20.13-CAN-27363-02
20. Standard test method for J_{IC}, a measure of fracture toughness. In: ASTM E813-81
21. Toffolon-Masclet C, Brachet J-C, Jago G (2002) J Nucl Mater 305:224–231
22. Delayed hydride cracking in zirconium alloys in pressure tube nuclear reactors, IAEA TECDOC 1410, Final report of a coordinated research project, 1998–2002, October 2004
23. Jovanovic MT, Eadie RL, Ma Y, Anderson M, Sagat S, Perovic V (2001) Mater Charact 47:259–268. doi:10.1016/S1044-5803(01)00179-6
24. Simpson LA, Cann CD (1984) J Nucl Mater 126:70–73. doi:10.1016/0022-3115(84)90533-6
25. Griffiths M, Winegar JE, Buyers A (2007) J Nucl Mater. doi:10.1016/j.jnucmat.2007.09.007
26. Benites GM, Fernández Guillermet A, Cuello GJ, Campo J (2000) J Alloys Compd 299:183–188. doi:10.1016/S0925-8388(99)00683-0
27. Griffiths M, Mecke JF, Winegar JE (1996) In: Bradley R, Sabol GP (eds) Zirconium in the nuclear industry: 11th international symposium, ASTM STP 1295, pp 580–602
28. Skinner BC, Dutton R (1990) In: Moody NR, Thompson A (eds) The minerals, metals and materials society. Pennsylvania, pp 73–83

29. Pan ZI, Ritchie IG, Puls MP (1996) J Nucl Mater 228:227–237. doi:10.1016/S0022-3115(95)00217-0
30. Carpenter GJC (1973) J Nucl Mater 48:264–266. doi:10.1016/0022-3115(73)90022-6
31. MacEwen SR, Coleman CE, Ells CE, Faber J Jr (1985) Acta Metall 33:753–757. doi:10.1016/0001-6160(85)90098-7
32. Shi S-Q, Puls MP (1999) J Nucl Mater 275:312–317. doi:10.1016/S0022-3115(99)00132-4
33. Shmakov AA (2004) At Energy 97(4):707–712. doi:10.1007/s10512-005-0051-7
34. Shek GF, Jovanovic MT, Seahra H, Li D, Eadie RL (1996) J Nucl Mater 231:221–230. doi:10.1016/0022-3115(96)00370-4
35. Jovanovic MT, Shek GF, Seahra H, Eadie RL (1998) Mater Charact 40:15–25. doi:10.1016/S1044-5803(97)00091-0